Low-temperature Argon Plasma Jet with Cascading Electrode Technique for Biological Applications

Hamid Ghomi (h-gmdashty@sbu.ac.ir)
Shahid Beheshti University
Pourya Seyfi
Shahid Beheshti University
Maryam Keshavarzi
Tarbiat Modares University
Saeed Zahedi
Shahid Beheshti University
Ahmad Khademi
Shahid Beheshti University

Article

Keywords:

Posted Date: April 12th, 2022

DOI: https://doi.org/10.21203/rs.3.rs-1517092/v1

Low-temperature Argon Plasma Jet with Cascading Electrode Technique for Biological Applications

Pourya Seyfi[1], Maryam Keshavarzi[2], Saeed Zahedi[1], Ahmad Khademi[1] and Hamid Ghomi[1]✉

[1] Laser and Plasma Research Institute, Shahid Beheshti University, Evin 1983963113, Tehran, Iran. [2] Department of Mechanical and Biosystems Engineering, Faculty of Agriculture, Tarbiat Modares University, Tehran, Iran. ✉ (E-mail: h-gmdashty@sbu.ac.ir)

In this study, the design, performance, and characteristics of a low-temperature argon plasma jet with cascading electrode technique (APJCE) are presented. APJCE is designed based on a tip-ring structure with a cascading ring. The effect of plasma jet driven by repetitive high-voltage microsecond pulses in APJCE structure was measured qualitatively in local surface temperature detection system. Then, by applying the generated plasma jet to biological surface and measuring and characterizing the electrical parameters, we obtained a plasma jet, which is electrically and thermally in the cold plasma regime. Simulation of the electric field distribution in the nozzle also yielded similar results to the experimental results. Finally, by cascading electrodes, we were able to guide the plasma column to the nozzle output so that the plasma temperature in four centimeter of the nozzle output is 37℃. The resulting plasma jets were studied by atomic emission spectroscopy and the intensity of the spectral lines of the atmospheric argon plasma jet spectra was obtained as a final experimental result at the output.

In the last decade, the use of new sciences and technologies and the application of these sciences in various industries such as agriculture, nanotechnology, nutrition and medicine have been considered by researchers, physicians and industrialists in the world.[1-5] One of the most important of these sciences is plasma and its important applications, which have been very important in the development of science.[3-7] The use of plasma properties in surface activation, hydrophilicity and hydrophobicity, ozone generation, air pollution reduction, treatment of diabetic wounds, skin repair, treatment of cancerous tumors and numerous other applications is possible by using various plasma generation structures.[4-13] In the meantime, the use of plasma instruments is of special importance due to its use in the synthesis of bio-surfaces as well as clinical tests.[4] Plasma jet is one of the most important plasma instruments used in this field.[12-16] Argon and helium plasma jets with different gas combinations are the most important instruments used in the field of bio plasma.[13-17] To plasma jets generate, various jet nozzle structures and power supplies with different electrical parameters can be used.[17,18] Structures such as tip, ring, tip -ring, ring-ring are used depending on the experimental conditions and parameters that are desired.[17,18] Also, variations in power supply parameters play a very important role in the results of plasma treatment.[17-19] The use of high voltage nanosecond pulses, high voltage pulses in radio and microwave frequencies, mixed electric field and variations in pulse width and applied voltage have been among the most important parameters that have been considered by researchers in this decade.[14,19] Another of the most basic variable parameters of plasma jets is gas and gaseous compounds used to generate plasma.[14-19] The generation of helium plasma jets is very easy due to the inherent properties of helium gas and plasma jets can also be generated by exciting a weak electric field.[16-19] But there are challenges to generating argon plasma jet that can be used in clinical experiments.[4-15] Creating streamers in the plasma column causes micro-discharge on the target and micro-discharge causes electric shocks on the target.[20,21] As a result of the micro-discharge colliding with the target surface, the surface temperature locally deviates significantly from the cold plasma temperature and damages the surface. Methods have been proposed by researchers to solve this problem. Using the microwave frequency as a source of plasma generation is one of the methods that generates low temperature argon plasma jets.[14] But the design and construction of nozzles, waveguides and microwave frequency sources have complexities that make access to this plasma source difficult for all researchers.[14] In this paper, we present a structure that can be used to ignite argon plasma jets with biological applications by medium frequency high voltage pulses.

Result

Figure 1 shows the actual image of the structure of the jet nozzle with the tip-ring method and with the cascade ring. This nozzle consists of a quartz tube with a diameter of 5 mm and a thickness of 0.8 mm. The tip-ring electrodes are made of copper wire with a diameter of 0.3 mm and are configured in different structures. A high voltage pulse power supply has been used to ignite argon gas in the jet nozzle and generate plasma jets. Figure 2 shows the pulse voltage and current diagram of the power supply used. High voltage pulse with an amplitude of 12 kV (Peak) and a pulse repetition frequency of 6 kHz is applied to the nozzle. Figure 3 shows the experimental schematic of APJCE set-up and measuring instruments.

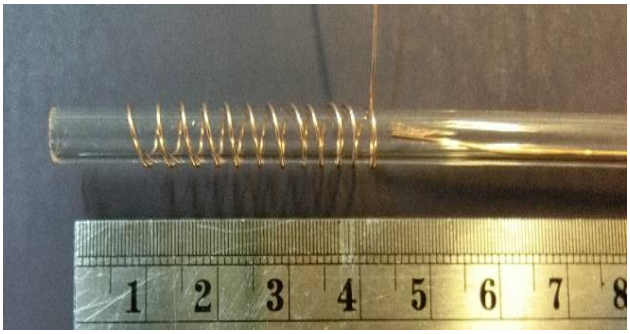

FIG. 1. Jet nozzle with tip-ring method (cascade ring).

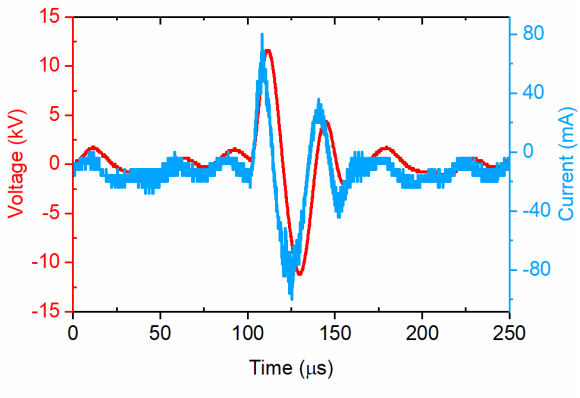

FIG. 2. The voltage and jet current waveforms

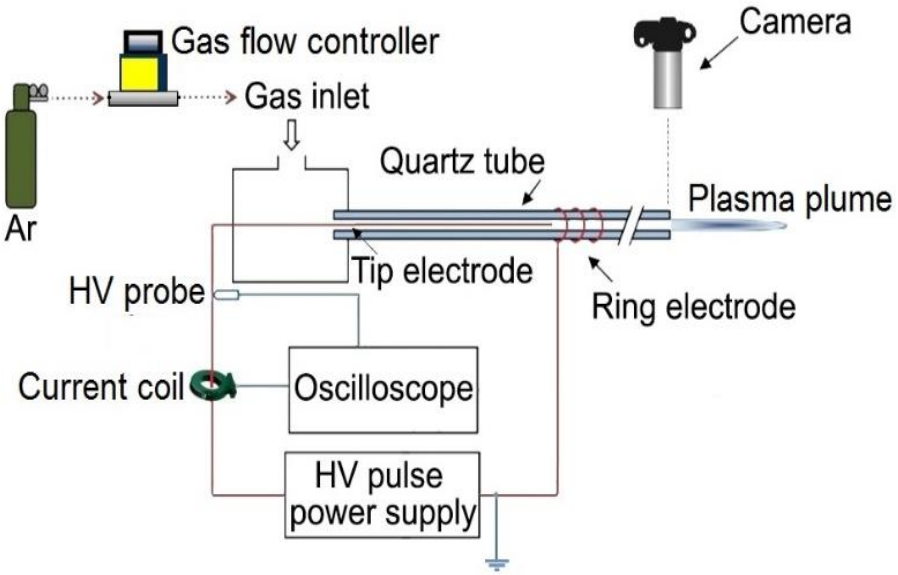

FIG. 3. The experimental schematic of APJCE set-up and measuring instruments

The following equations are used to calculate the average electrical power applied to the plasma jet. Where P_{ave} and $P(t)$ are the average and time-dependent electrical power, respectively, E_{pulse} is the energy per pulse, $V(t)$ and $I(t)$ are the time-dependent voltage and current, respectively. Average electrical power is assumed to be constant (20 watt) in all measurements and treatments.

$$\boldsymbol{P}(\boldsymbol{t}) = \boldsymbol{V}(\boldsymbol{t}) \times \boldsymbol{I}(\boldsymbol{t}) \quad (1)$$

$$\boldsymbol{E_{pulse}} = \int_{0}^{T} \boldsymbol{P(t)dt} \quad (2)$$

$$\boldsymbol{P_{ave}} = \frac{\boldsymbol{E_{pulse}}}{\boldsymbol{T}} \quad (3)$$

Now we want to examine the experimental results. In the experimental conditions, we obtained the plasma jet of Figure 4 with 12 turns of the cascade ring electrode.

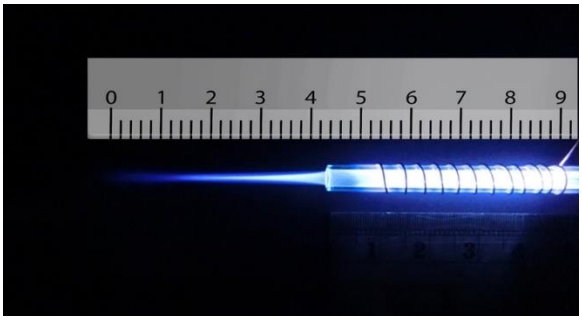

FIG. 4. Argon plasma jet with APJCE structure

As shown in Figure 4, the plasma plume is guided approximately 4 cm out of the jet nozzle outlet. In this structure, a 12-turn ring electrode is connected to the jet nozzle at the intervals reported in Figure 9. The output obtained is the most optimal result compared to other structures, which we will analyze and compare in the following. But at this stage the APJCE is analyzed for local temperature and electric shock. The temperature distribution on the target surface was measured by Fluke VT04A Visual IR Thermometer. Thermal image Figure 5 shows the thermal effects of a plasma jet colliding with a finger. The thermal image in Figure 6 was used to compare the temperature in which the plasma jet did not collision the finger. This comparison shows that the plasma jet increase the local of collision temperature by only 1℃.

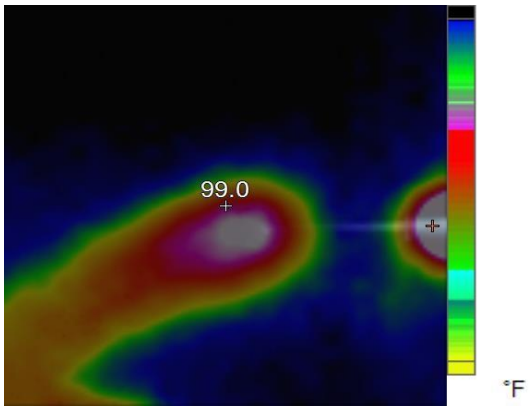

FIG. 5. Thermal image of APJCE colliding with finger

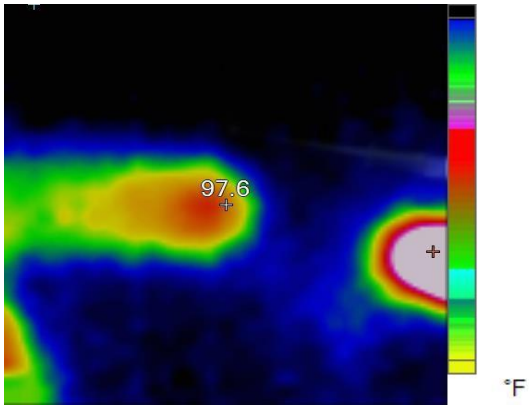

FIG. 6. Thermal image of the finger as a reference

Thermal images show that the surface temperature after contact with the plasma has risen from 36℃ to 37℃ and this temperature is in the range of cold plasma. Atomic emission spectroscopy has been used to evaluate the accuracy of APJCE performance and plasma parameters. The intensity of the species in the plasma jet can be seen in Figure 7. To investigate possible electric shocks, we used a biological target with approximate characteristics to the human body. For these experiments, the liver is used, as you can see in the structure in Figure 8, to perform experimental tests of electric shocks caused by argon plasma jets and surface temperatures in various structures.

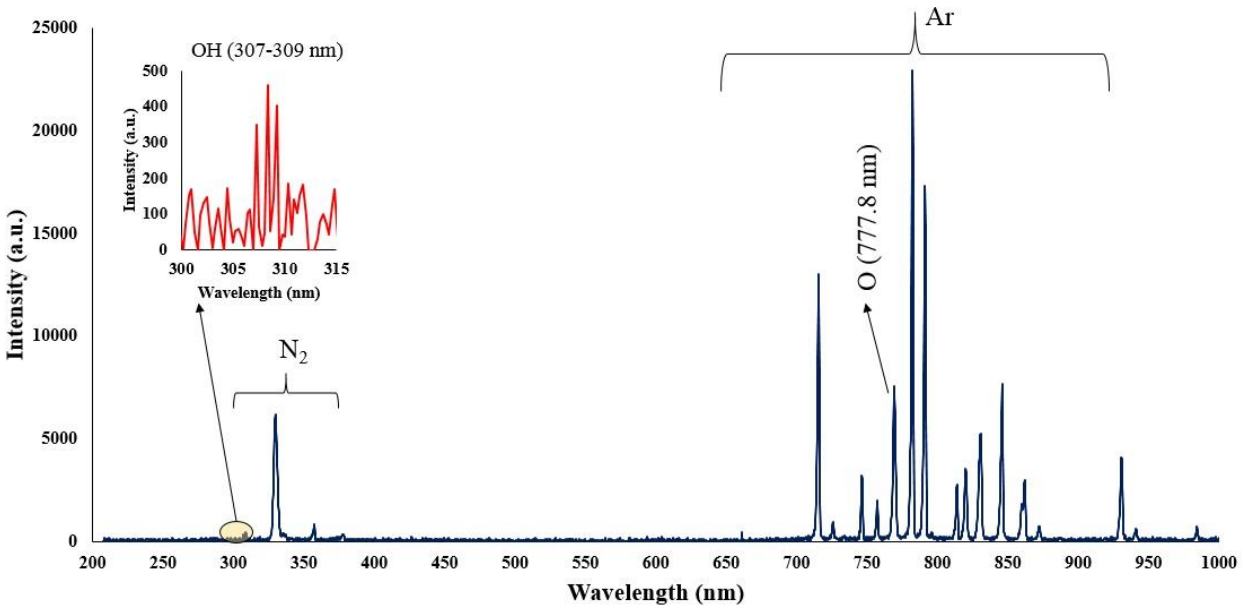

FIG. 7. The OES of plasma jet (APJCE) at 1 cm away from the jet tube.

The nitrogen molecules, argon, OH and oxygen atoms spectral lines are observed in figure 7. The emission spectrum of the plasma jet obtained in this study is similar to the emission spectrum of the argon plasma jet at atmospheric pressure.[22] In this plasma jet emission spectrum, high-intensity peaks were related to excited argon species observed in the range of 700 to 955 nm wavelength. The atomic emission spectrum of oxygen O* was also observed at 777 nm. The lowest intensity peaks correspond to the OH spectrum in the range of 307 to 309 nm. Nitrogen excited species were observed in the range of 310 to 430 nm. At this stage, other structures are investigated and finally compared. Figure 9 shows the different structures we have used for comparison. This figure is a cross section of different structures of plasma jet nozzles.

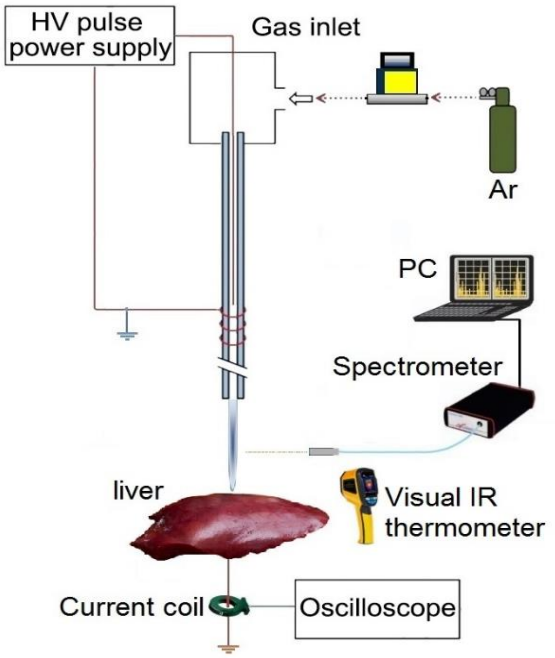

FIG. 8. Experimental schematic of APJCE Irradiation with surface and measurements of electric shock and thermal effects results.

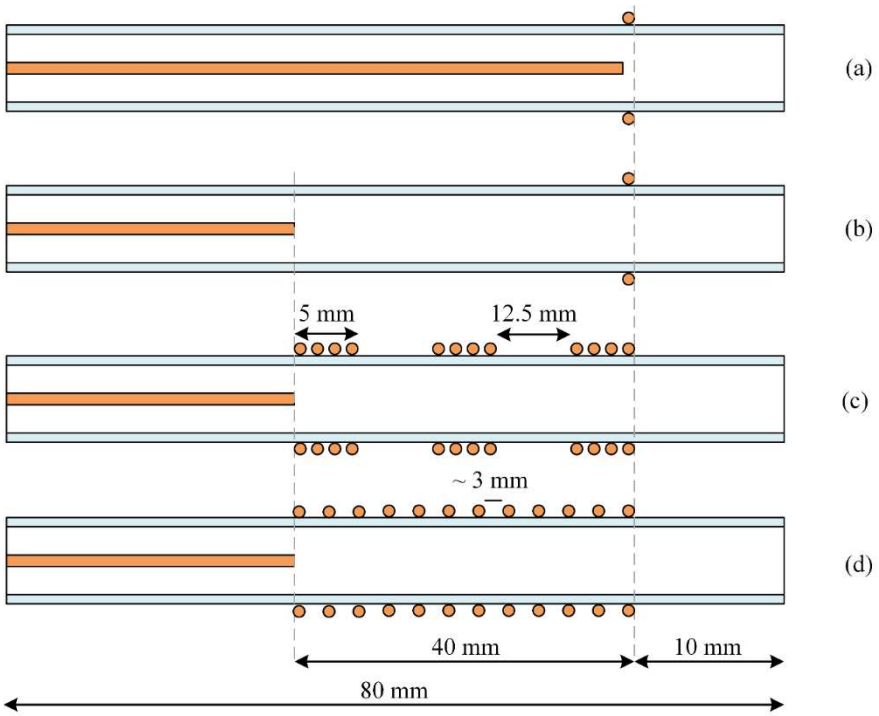

FIG. 9. Different structures of plasma jet nozzles, (a)Tip-Ring1, (b)Tip-Ring2, (c)Tip-Ring-Cascading1, (d)Tip-Ring-cascading2

With equal electrical conditions, we study the plasma jet and its performance in different structures. To deeply understand the performance of different nozzles, we first simulate the performance of the nozzles according to the nozzle structure of Figure 9. According to this simulation, the average electric field from the tip to the end of the jet tube is calculated and plotted. The side view of the 2D simulation of average electric field of the plasma jet nozzle in the direction of the nozzle length is shown in figures 10-14. The electric field propagated in a quartz tube can be calculated based on the following equations:

$$\boldsymbol{E} = -\boldsymbol{\nabla}\phi \quad (4)$$

$$\boldsymbol{\nabla^2}\phi = \rho \quad (5)$$

$$\boldsymbol{D} = \varepsilon_0\varepsilon_r\boldsymbol{E} \quad (6)$$

$$\boldsymbol{\nabla}.\boldsymbol{J} = -\frac{\partial\rho}{\partial t} \quad (7)$$

$$\boldsymbol{J} = \sigma\boldsymbol{E} + \frac{\partial\boldsymbol{D}}{\partial t} + \boldsymbol{J_e} \quad (8)$$

The parameters in the formulas refer to the following definitions.

$\boldsymbol{E}$ is the electric field intensity, ϕ is the electric potential, ρ is the electric charge density, $\boldsymbol{D}$ is the electric displacement, ε_0 is the permittivity of free space, ε_r is the relative permittivity, $\boldsymbol{J}$ is the total current density, σ is the electrical conductivity and, $\boldsymbol{J_e}$ is the externally generated current density.[23,24] The boundary conditions for the electric potential are considered as follows and the calculations are performed accordingly. In the definition of time-dependent variables, the applied voltage to the tip electrode is defined as $\phi_t = V_1(t)$ and oscillates according to Figure 2, and the applied potential to the ring electrode is defined as $\phi_r = 0$. Boundary conditions at the interface between the two medias are expressed as follows:

$$\boldsymbol{n} \times (\boldsymbol{E_1} - \boldsymbol{E_2}) = 0 \quad (9)$$

$$\boldsymbol{n}.(\boldsymbol{D_1} - \boldsymbol{D_2}) = \rho \quad (10)$$

$$\boldsymbol{n}.(\boldsymbol{J_1} - \boldsymbol{J_2}) = -\frac{\partial\rho}{\partial t} \quad (11)$$

In the above equations n is the normal surface vector. The simulated electric field between the tip electrodes and end of plasma jet tube, based on the above-mentioned equations and boundary conditions, were performed and the results are shown in figures 10-13. The average value of the electric field across the tip and outlet boundaries is given by

$$(norm\,E)_{ave} = \frac{1}{T} \times \frac{1}{D} \int\int E(s,t)\,dsdt \quad (12)$$

Which T is period time, D is arc length, and s is integral orientation.

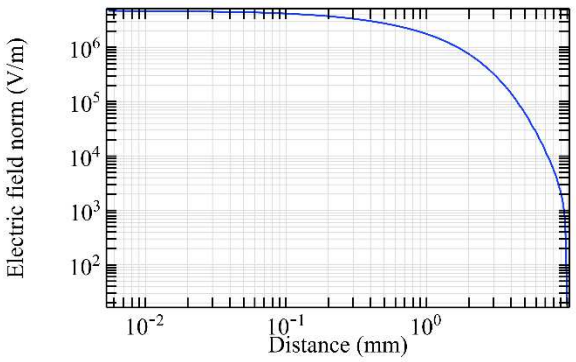

FIG. 10. Simulation of electric field from tip electrode to end of plasma jet nozzle based on nozzle Figure 9(a).

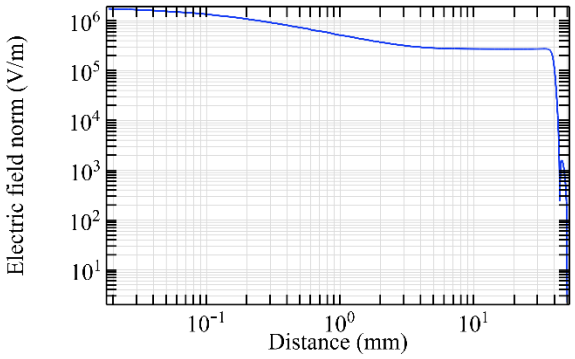

FIG. 11. Simulation of electric field from tip electrode to end of plasma jet nozzle based on nozzle Figure 9(b).

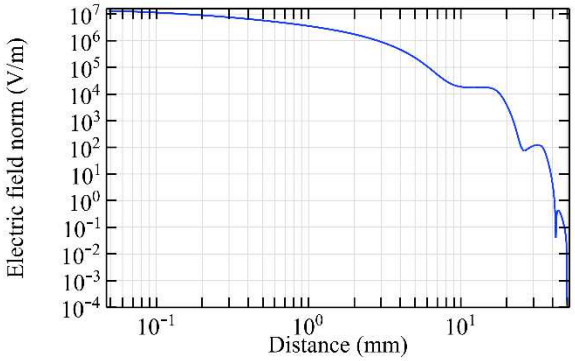

FIG. 12. Simulation of electric field from tip electrode to end of plasma jet nozzle based on nozzle Figure 9(c).

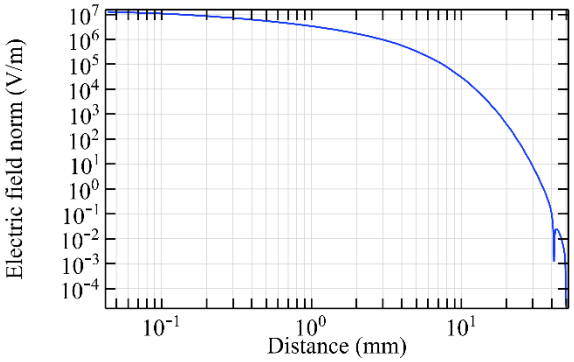

FIG. 13. Simulation of electric field from tip electrode to end of plasma jet nozzle based on nozzle Figure 9(d).

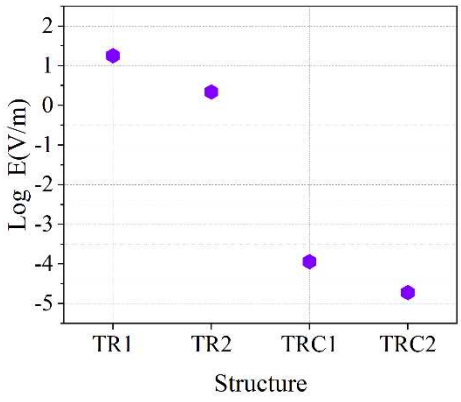

FIG. 14. Comparison of electric field at the end of the tube in different structures of plasma jet nozzles.

By studying the diagram in Figure 10, we can see the decreasing trend of the electric field from the tip to the end of the jet nozzle. The decrease rate of the electric field in Figure 11, decreases with a different trend. This variation is due to the distance between the tip electrode and the ring electrode. In the Figure 12 diagram, there is a fluctuation in the electric field. The fluctuation is caused by the structure of the ring electrode. Finally, in Figure 13, the fluctuations in the previous structure are eliminated. But the important point is that while the trend of electrical field variations in all structures has a decreasing trend, the average electric field at the end of the jet tube is different in four structures. The variations mentioned above can be seen in Figure 14. As can be seen in the diagram, in the two structures TR1 and TR2, the electric field at the end of the jet tube has a higher intensity than the structures TRC1 and TRC2. In this step, we examine the simulated structures experimentally and then compare them with each other. The results are reported in Figure 15.

FIG. 15. Comparison of plasma jet lengths according to the structures of Figure 9.

The results of plasma jet length show that we can have acceptable jet length in both Tip-Ring and Tip-Ring-Cascading structures. In TR1 structure, the maximum length of plasma jet with a length of more than 5 cm is obtained. After TR1 structure, TRC2 with a plasma jet length of more than 4 cm is obtained. The TRC2 structure has the longest plasma jet length after the TR1 structure. In the TR2 structure, a plasma jet is give out with a length of 1 cm from the tube outlet. But in the structure of TRC1 the plasma jet is very weak and the plasma column is not formed properly at the outlet of the nozzle tube. Comparison of simulation results and experimental results in TR1, TR2 and TRC1 can largely confirm each other's final results. But in TRC2, unlike the lowest electric field at the end of the jet tube, a 4 cm length plasma jet is obtained at the outlet. Creating proper symmetry and distance in the cascade electrode rings causes the plasma column to be transferred from the tip electrode to the end of the jet tube and then propagated with a suitable length out of the jet nozzle. Asymmetry in the ring electrode impairs the performance of the cascade electrode. TRC1 represents an asymmetric cascade electrode that failed to properly transfer plasma to the outlet, and the plasma column in the nozzle is greatly damped, and at the nozzle output we see a weak column of the plasma afterglow. At this step, plasma jets in TR1 and TRC2 structures, which are acceptable structures in terms of plasma jet length, were subjected to experimental tests of electric shock and surface thermal degradation. Figure 16 shows the total electric current caused by the collision of a plasma jet with the surface. This electric current is related to the structure of TR1 and is measured according to the schematic of Figure 8.

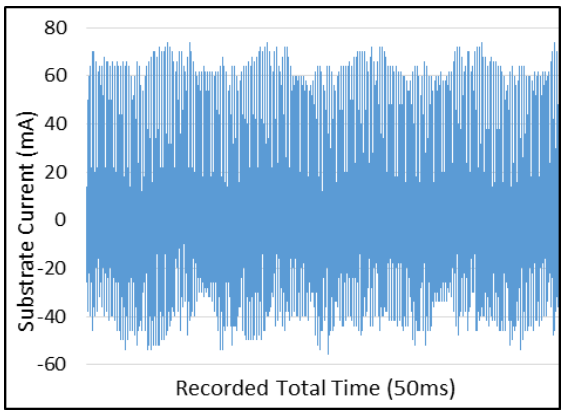

FIG. 16. Substrate current, while the TR1 plasma jet collides the target.

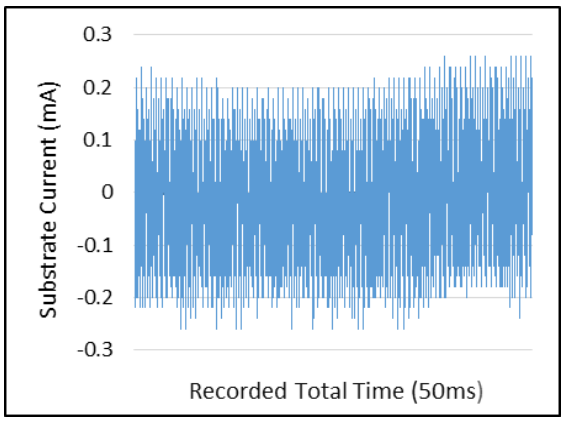

FIG. 17. Substrate current, while the TRC1 plasma jet collides the target.

As shown in Figure 16, the peak range of electric current pulses is in the range of 60 mA, and this range is in the scope of the pulse power supply current. These conditions indicate that the plasma column could not reach the acceptable ohmic resistance to prevent electric shocks. In Figure 17, however, the peak range of electric current is in the range of 200 µA. By investigating the electric current of the substrate in the TRC2 structure, it can be concluded that in this structure, in terms of the electrical circuit, the plasma generation unit, ie the high voltage power supply, is isolated from the generated plasma jet. In this structure, electric shock is not applied to the target and only the plasma jet collides the surface with all the species generated. Finally, the temperature of the area where the plasma jet collides with the surface is measured and compared in two structures. The results of temperature measurements are reported in Figure 18.

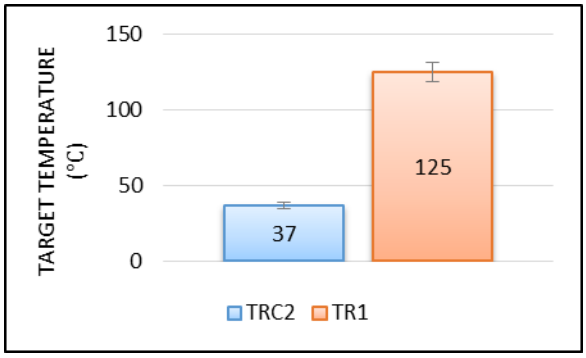

FIG. 18. Plasma jet collision zone temperature with target surface in TR1 and TRC2 structures.

The results clearly show that plasma jets generated with TR1 structure can cause severe thermal degradation of biological surfaces. But in comparison, if we use the TRC2 structure to generate plasma jets, the surface temperature will increase by only 1℃ compared to room temperature. Finally, we obtain a cold argon plasma jet capable of treating biological surfaces.

Summary

Based on the presented results, a new method for generating argon plasma jets for biological applications has been proposed. With the new structure of the jet nozzle and the design of the new electrode structure, we were able to achieve a plasma jet without electric shock and thermal degradation of the surface in a simple yet very precise method. Generation and transfer of plasma jet by cascading electrode method to the structure allows, the output plasma jet to be electrically isolated from the source of plasma generation.

Methods

A jet nozzle structure is designed with two electrodes, the electrode inside the tube as the igniter and the outer electrode as the controller of the plasma column. The inner electrode is designed as a tip and the outer electrode is designed as a cascading ring. The power supply used is a high voltage resonant pulse generating circuit designed in flyback mode. Figure 19 shows the circuits' used.[25]

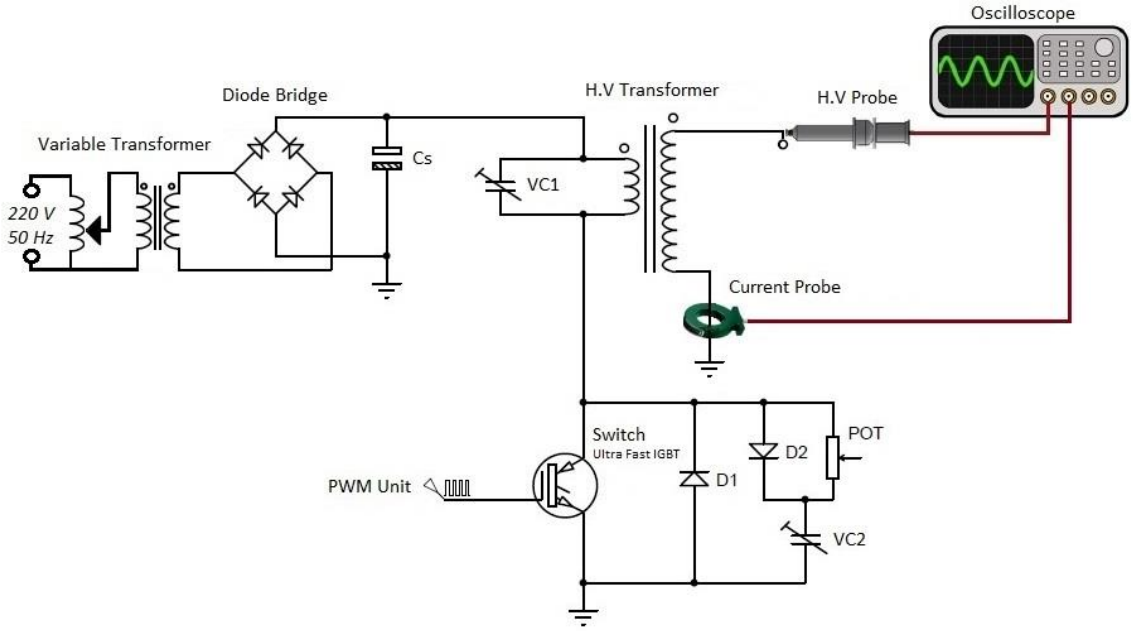

FIG. 19. Pulsed High Voltage Power Supply Circuit.

The mass flow controller are employed to provide constant Ar flow (99.999%) , which Located in the path of the argon bottle and the gas inlet of the jet system. Gas adjustment is done by Harris Argon 355-2 Flowmeter Regulator. Besides, the Ar gas flow rate is 8 Lit/min (133 cm3.s-1) in all measurements. The length of the plasma jet is recorded by a Casio high-speed Exilim Ex-ZR700 Digital Camera. The voltage and the current are measured by a high voltage probe (TEKTRONIX P6015 1:1000) and a current probe (rogowski coil) [26], respectively. The electrical signals are visualized using a TEKTRONIX TDS 2024B oscilloscope (200 MHz). The Optical Emission Spectrometer (OES) with model HR 2000 was used to detect the species in plasma jet. The spectroscopy from the plasma jet was measured at a distance of one centimeter radially and two centimeters longitudinally where the plasma jet hit the surface.

References

1. Shashurin, A., M. N. Shneider, A. Dogariu, R. B. Miles, and M. Keidar. "Temporal behavior of cold atmospheric plasma jet." *Applied Physics Letters* 94, no. 23, 231504, (2009).
2. Chauvin, Julie, Florian Judée, Mohammed Yousfi, Patricia Vicendo, and Nofel Merbahi. "Analysis of reactive oxygen and nitrogen species generated in three liquid media by low temperature helium plasma jet." *Scientific reports* 7, no. 1, 1-15, (2017).
3. Nicol, McKayla J., Timothy R. Brubaker, Brian J. Honish, Alyssa N. Simmons, Ali Kazemi, Madison A. Geissel, Connor T. Whalen et al. "Antibacterial effects of low-temperature plasma generated by atmospheric-pressure plasma jet are mediated by reactive oxygen species." *Scientific reports* 10, no. 1, 1-11, (2020).
4. Laroussi, Mounir, and XinPei Lu. "Room-temperature atmospheric pressure plasma plume for biomedical applications." *Applied Physics Letters* 87, no. 11,113902, (2005).
5. Ambrico, Paolo F., Milan Šimek, Caterina Rotolo, Massimo Morano, Angelantonio Minafra, Marianna Ambrico, Stefania Pollastro, Donato Gerin, Francesco Faretra, and Rita M. De Miccolis Angelini. "Surface Dielectric Barrier Discharge plasma: a suitable measure against fungal plant pathogens." *Scientific Reports* 10, no. 1, 1-17, (2020).
6. Güner, Mehmet Haşim, Tahsin Görgülü, Abdulkerim Olgun, Merve Torun, and Eksal Kargi. "Effects of ozone gas on skin flaps viability in rats: an experimental study." *Journal of Plastic Surgery and Hand Surgery* 50, no. 5, 291-297, (2016).
7. Conrads, H., and M. Schmidt. "Plasma generation and plasma sources." *Plasma Sources Science and Technology* 9, no. 4, 441, (2000).
8. Walsh, James L., J. J. Shi, and Michael G. Kong. "Contrasting characteristics of pulsed and sinusoidal cold atmospheric plasma jets." *Applied Physics Letters* 88, no. 17, 171501, (2006).
9. Kim, Sun Ja, and T. H. Chung. "Cold atmospheric plasma jet-generated RONS and their selective effects on normal and carcinoma cells." *Scientific reports* 6, no. 1, 1-14, (2016).
10. Bormashenko, Edward, Roman Grynyov, Yelena Bormashenko, and Elyashiv Drori. "Cold radiofrequency plasma treatment modifies wettability and germination speed of plant seeds." *Scientific reports* 2, no. 1, 1-8, (2012).
11. Khlyustova, Anna, Cédric Labay, Zdenko Machala, Maria-Pau Ginebra, and Cristina Canal. "Important parameters in plasma jets for the production of RONS in liquids for plasma medicine: A brief review." *Frontiers of Chemical Science and Engineering* 13, no. 2, 238-252, (2019).
12. Laroussi, Mounir, and Tamer Akan. "Arc-free atmospheric pressure cold plasma jets: A review." *Plasma Processes and Polymers* 4, no. 9, 777-788, (2007).
13. Li, Xuechen, Jiacun Wu, Boyu Jia, Kaiyue Wu, Pengcheng Kang, Furong Zhang, Na Zhao, Pengying Jia, Long Wang, and Shouzhe Li. "Generation of a large-scale uniform plasma plume through the interactions between a pair of atmospheric pressure argon plasma jets." *Applied Physics Letters* 117, no. 13, 134102, (2020).
14. Fu, Wenjie, Chaoyang Zhang, Cong Nie, Xiaoyun Li, and Yang Yan. "A high efficiency low-temperature microwave-driven atmospheric pressure plasma jet." *Applied Physics Letters* 114, no. 25, 254106, (2019).
15. Shashurin, A., and M. Keidar. "Experimental approaches for studying non-equilibrium atmospheric plasma jets." *Physics of Plasmas* 22, no. 12,122002, (2015).
16. Jiang, Jingkai, and Peter J. Bruggeman. "Absolute ion density measurements in the afterglow of a radiofrequency atmospheric pressure plasma jet." *Journal of Physics D: Applied Physics* 54, no. 15,15LT01, (2021).
17. Breden, Doug, Kenji Miki, and Laxminarayan L. Raja. "Computational study of cold atmospheric nanosecond pulsed helium plasma jet in air." *Applied Physics Letters* 99, no. 11, 111501, (2011).
18. Seo, Young Sik, Abdel-Aleam H. Mohamed, Kyung Chul Woo, Hyun Wook Lee, Jae Koo Lee, and Kyong Tai Kim. "Comparative studies of atmospheric pressure plasma characteristics between He and Ar working gases for sterilization." *IEEE transactions on plasma science* 38, no. 10, 2954-2962, (2010).
19. Boselli, Marco, Vittorio Colombo, Matteo Gherardi, Romolo Laurita, Anna Liguori, Paolo Sanibondi, Emanuele Simoncelli, and Augusto Stancampiano. "Characterization of a cold atmospheric pressure plasma jet device driven by nanosecond voltage pulses." *IEEE Transactions on Plasma Science* 43, no. 3, 713-725, (2015).
20. Sands, Brian L., Biswa N. Ganguly, and Kunihide Tachibana. "A streamer-like atmospheric pressure plasma jet." *Applied Physics Letters* 92, no. 15,151503, (2008).
21. Pinchuk, M. E., O. M. Stepanova, Mikhail Gromov, Ch Leys, and Anton Nikiforov. "Variation in guided streamer propagation along a DBD plasma jet by tailoring the applied voltage waveform." *Applied Physics Letters* 116, no. 16,164102, (2020).
22. Akatsuka, Hiroshi. "Optical Emission Spectroscopic (OES) analysis for diagnostics of electron density and temperature in non-equilibrium argon plasma based on collisional-radiative model." *Advances in Physics: X* 4, no. 1, 1592707, (2019).
23. Polo Jr, John A., and Akhlesh Lakhtakia. "Surface electromagnetic waves: a review." *Laser & Photonics Reviews* 5, no. 2,234-246, (2011).

24. Kristensson, Gerhard. "Transient electromagnetic wave propagation in waveguides." *Journal of Electromagnetic Waves and Applications* 9, no. 5-6, 645-671, (1995).
25. Seyfi, Pourya, Saeed Zahedi, Hojat Shojaei, and Hamid Ghomi. "Investigation of the effects of mixed electric field stress on high voltage transformer insulation." *Electrical Engineering*, 1-13, (2022).
26. Argüeso, M., G. Robles, and J. Sanz. "Measurement of high frequency currents with a Rogowski coil." *Rev. Sci. Instrum* 76, no. 6, 65101-65107, (2005).

Acknowledgements

The authors would like to thank Dr. Hamid Ghomi at laser and plasma research institute, for his guidance and generous support for this project.

Author Contributions

Pourya Seyfi Prepared the main body of manuscript, collected the data, was the originator of this article.and contributed to the interpretation of data. Maryam Keshavarzi has performed optical emission spectroscopy and also analyzed the relevant information. Saeed Zahedi has performed the measurement and analysis of electrical parameters of the high voltage power supply. Ahmad Khademi has performed the electric field simulation in plasma jets and related results. Hamid Ghomi Contributed to the conception and design of the work, interpretation of data and supervised the project. All authors discussed the results and contributed to the final manuscript.

Competing Interests: The authors declare no competing interests.

Correspondence and requests for materials should be addressed to Hamid Ghomi. The datasets used and/or analysed during the current study available from the corresponding author on reasonable request.